AGU PUBLICATIONS

JGR

Journal of Geophysical Research: Atmospheres

RESEARCH ARTICLE
10.1002/2016JD025401

Key Points:
- A multiscale network of land-air flux comprehensive observation sites has been implemented for the first time on the TP in TIPEX III
- Here we place great emphasis on land surface parameters and turbulence characteristics on the TP and surrounding region

Correspondence to:
Y. Wang,
pbl_wyj@sina.cn

Citation:
Wang, Y., et al. (2016), Analysis of land surface parameters and turbulence characteristics over the Tibetan Plateau and surrounding region, *J. Geophys. Res. Atmos.*, *121*, 9540–9560, doi:10.1002/2016JD025401.

Received 24 MAY 2016
Accepted 29 JUL 2016
Accepted article online 31 JUL 2016
Published online 31 AUG 2016

Analysis of land surface parameters and turbulence characteristics over the Tibetan Plateau and surrounding region

Yinjun Wang[1], Xiangde Xu[1], Huizhi Liu[2], Yueqing Li[3], Yaohui Li[4], Zeyong Hu[5], Xiaoqing Gao[5], Yaoming Ma[6], Jihua Sun[7], Donald H. Lenschow[8], Shiyuan Zhong[9], Mingyu Zhou[10,11], Xindi Bian[12], and Ping Zhao[1]

[1]Chinese Academy of Meteorological Sciences, Beijing, China, [2]LAPC, Institute of Atmospheric Physics, Chinese Academy of Sciences, Beijing, China, [3]Institute of Plateau Meteorology, China Meteorological Administration, Chengdu, China, [4]Key Laboratory of Arid Climatic Change and Reducing Deserter of Gansu Province, Institute of Arid Meteorology, China Meteorological Administration, Lanzhou, China, [5]Cold and Arid Regions Environmental and Engineering Research Institute, Chinese Academy of Sciences, Lanzhou, China, [6]Key Laboratory of Tibetan Environment Changes and Land Surface Processes, Institute of Tibetan Plateau Research, Chinese Academy of Sciences, Beijing, China, [7]Meteorological Institute of Yunnan Province, Kunming, China, [8]National Center for Atmospheric Research, Boulder, Colorado, USA, [9]Michigan State University, East Lansing, Michigan, USA, [10]National Marine Environmental Forecasting Center, Beijing, China, [11]National Climate Center, China Meteorological Administration, Beijing, China, [12]Northern Research Station, USDA Forest Service, East Lansing, Michigan, USA

Abstract Based on the results from 11 flux sites during the third Tibetan Plateau (TP) Experiment (TIPEX III), land surface parameters and the turbulence characteristics of the atmospheric surface layer over the TP and surrounding region are analyzed. Monin-Obukhov similarity theory has been used to calculate the aerodynamic roughness length z_{0m} and the excess resistance to heat transfer $kB^{-1} = \ln(z_{0m}/z_{0h})$, and the factors that cause variations of z_{0m} and kB^{-1} are investigated. The main drivers for the diurnal variations of surface albedo (α) at different sites are solar elevation, solar radiation, and soil moisture. The eddy correlation method is utilized to inversely calculate bulk transfer coefficients for momentum (C_D) and heat (C_H) at different sites. The relationships between C_D and C_H and the wind speed at 10 m follow a power law for unstable stratification. For stable stratification, both C_D and C_H increase with increasing wind speed when wind speed is less than 5 m/s. Diurnal variations of turbulent fluxes are compared at different sites, and the relationships between turbulent fluxes and other variables are analyzed. Wind speed variance normalized by the friction velocity ($\sigma_u/u_*, \sigma_v/u_*, \sigma_w/u_*$) for neutral stratification (C_{u1}, C_{v1}, C_{w1}), and temperature and humidity variance normalized by a temperature and humidity scale ($\sigma_T/T_*, \sigma_q/q_*$) under free convection ($z/L < -0.1$) (C_T, C_q) are fitted with similarity relations. The differences in similarity constants (C_{u1}, C_{v1}, C_{w1}, C_T, C_q) at different sites are discussed. For stable stratification, cases are divided into weakly stable conditions and intermittent turbulence, and the critical values for these two states are determined. Shear and buoyancy terms in the turbulence kinetic energy equation for different stratifications are analyzed.

1. Introduction

The Tibetan Plateau (TP), which has been called "the third pole" and "the world's water tower," plays an important role in the global climate and energy-water cycle [*Xu et al.*, 2008]. The TP has a large area, an average altitude above 4000 m and a land surface that absorbs a large fraction of incoming solar radiation. Thus, in summer the TP is a unique strong heat source in the middle troposphere and the resulting thermal structure leads to dynamic processes that transfer moist air in two steps up the plateau. This is similar to the conditional instability of the second kind mechanism of tropical cyclones [*Xu et al.*, 2014]. The thermodynamic and dynamic effects of the TP have great impact on weather and climate in eastern Asia, and land-air physical processes are one of the important factors. As a result, many recent studies have focused on the land-air interaction over the TP and China organized the first Qinghai-Xizhang Plateau Meteorological Experiment (QXPMEX) from May to August 1979 [*Zhang et al.*, 1988]. Several surface and sounding stations and six heat source stations were deployed on the TP, and surface radiation, thermal balance, and heat source characteristics were revealed as a result of QXPMEX. However, atmospheric sounding technology was relatively backward in the late 1970s and there were only a few sites over the TP. Furthermore, the lack of fast response measurements precluded accurate flux measurement. As a result, the second Tibetan Plateau Experiment (TIPEXII) set up three flux

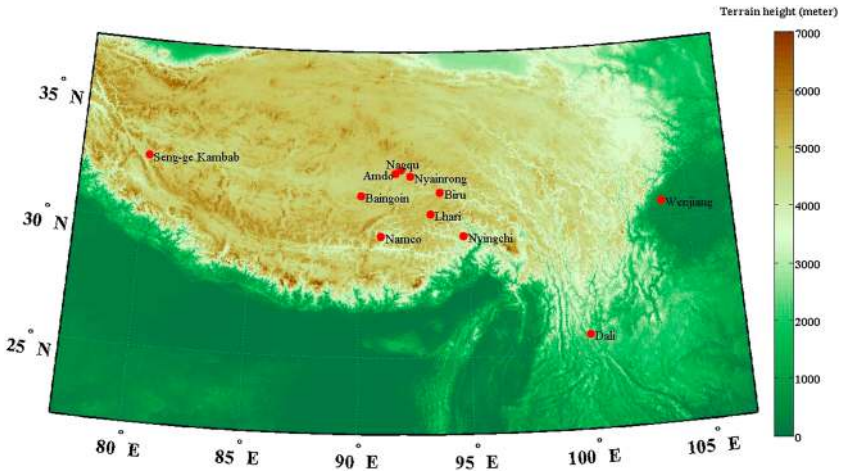

Figure 1. Locations of the 11 sites used in this paper on the Tibetan Plateau.

observational sites over the TP for the first time from May to August 1998. From west to east, Garze, Damxung, and Qamdu are representative of the following climates: dry and alpine desert in the western TP, a semiarid transition zone in the middle TP, and a humid valley in the eastern TP, each with different land surface parameters and turbulence characteristics [*Zhou et al*., 2000]. Fast response measurements were obtained in TIPEXII, but the flux observational sites were sparse and observation periods were short. More observational data are needed to validate and improve the simulated results of land surface models over the TP.

Because of these limitations, the third Tibetan Plateau Experiment for atmospheric sciences (TIPEX III) has been organized by China Meteorological Administration since June 2013, a number of Chinese scientific research institutions and universities (e.g., the Chinese Academy of Meteorological Sciences, the Institute of Atmospheric Physics of CAS, Institute of Plateau Meteorology, Institute of Tibetan Plateau Research of CAS, Nanjing University of Information Science and Technology, and Peking University) participate in TIPEX III. The overall goals of TIPEX III are as follows: (1) generate a reanalysis data set that includes both remote sensing and surface observations, (2) elucidate energy, mass, and water cycling processes over the TP and develop a theory of how they influence the weather and climate over eastern Asia, and (3) improve the reliability of numerical simulation over the TP and the surrounding complex terrain. In order to fulfill the overall goals mentioned above, TIPEX III includes the observational experiments about multiple subfields of atmosphere (e.g., encrypted soundings observation during the monsoon processseason, cloud physics observations during the disastroussevere weather process, land-air interaction observations, and atmospheric hydrology observations). The scientific purpose goal of this manuscript mainly focuses on land-air interaction that which is one of the goals in TIPEX III. A multiscale network of land-air flux comprehensive observation sites has been implemented for the first time on the TP in TIPEX III by a number of Chinese scientific research institutions including (the Chinese Academy of Meteorological Sciences, the Institute of Atmospheric Physics of CAS, and the Institute of Tibetan Plateau Research of CAS). Although some other previous studies have quantified land surface parameters and surface layer turbulence characteristics using fast response measurements over different regions of the TP and its surroundings [*Shimizu*, 2015; *Zhang et al*., 2002; *Zhou et al*., 2005], there were deficiencies in these multisite analyses, especially those that are located within a relative small region of complex terrain. In TIPEX III 11 sites were set up within a "large network" that covers the TP and surrounding region. Site density was increased around Nagqu and five sites (Baingoin, Namco, Amdo, Nagqu, and Nyainrong) on the middle of the TP and two sites (Lhari and Biru) in the eastern TP were set up within "small network" (a rectangle stretching 350 km from north to south and 250 km from east to west). Four other sites were set up at Seng-ge Kambab in western TP, Nyingchi on the southern slopes of the TP, Dali on the southeastern TP edge, and Wenjiang on the Chengdu plain as shown in Figure 1. Tables 1 and 2 show the geographical and the fast/slow response sensor information for the 11 flux observational sites, respectively. One of the "large network" goals is to increase understanding of the variation of land surface parameters and surface layer turbulence characteristics. The similarity and representativeness of the sites around Nagqu are clarified by the "small network." Multisite comprehensive analysis would also allow an objective evaluation

Table 1. Geographical Conditions Represented by the 11 Tibetan Plateau and Surrounding Region Sites Used in This Study

Site Location	Longitude and Latitude	Elevation (m)	Land-Cover Type	Canopy Height (cm)
Amdo	91.6°E, 32.2°N	4695	alpine steppe	3
Seng-ge Kambab	80.1°E, 32.5°N	4350	bare soil with few obstacles	0
Baingoin	90.1°E, 31.4°N	4700	alpine steppe	4
Biru	93.7°E, 31.5°N	4408	alpine steppe	5
Dali	100.2°E, 25.7°N	1991	paddy cropland with few obstacles	80
Lhari	93.2°E, 30.7°N	4500	alpine meadow with few obstacles	15
Nyingchi	94.7°E, 29.8°N	3327	alpine meadow with few shrubs and trees	20
Namco	91.0°E, 29.8°N	4730	alpine steppe	7
Nagqu	91.9°E, 32.4°N	4509	alpine steppe	4
Nyainrong	92.3°E, 32.1°N	4730	alpine steppe	4
Wenjiang	103.8°E, 30.7°N	530	paddy cropland with few obstacles	70

of the accuracy of the grid data. Turbulent flux calculated by the eddy covariance method at the multisites is an important basis for evaluating the quality of reanalysis data. Such data can also be used to establish a climatology of land surface parameters in such a region. Additionally, testing an offline land surface parameterization scheme needs this kind of standard observational data.

Here we place great emphasis on land surface parameters and turbulence characteristics on the TP and surrounding region. Two important land surface parameters, the roughness length z_{0m} and the excess resistance to heat transfer kB^{-1}, are calculated using Monin-Obukhov similarity theory [*Yang et al.*, 2007] due to lack of high quality multiheight wind speed data at some sites. Surface albedo is an important variable

Table 2. Sensor and Data Sampling Characteristics for the 11 Sites Used in This Study

	Fast Response Measurements for (Sonic Anemometer and Gas Analyzer)[a]			
Site Location	Height (m)	North Offset (deg)	Acquisition Frequency (Hz)	Dates of Data Used
Amdo	2.98	270	10	07/15/2014–09/06/2014
Seng-ge Kambab	5	0	10	07/01/2014–09/15/2014
Baingoin	2.1	115	10	07/12/2014–09/03/2014
Biru	2	115	10	07/28/2014–09/14/2014
Dali	5.08	56	10	06/30/2014–09/05/2014
Lhari	2	140	10	07/26/2014–09/16/2014
Nyingchi	3.04	282	10	08/02/2014–10/02/2014
Namco	3.06	200	10	07/18/2014–07/31/2014
				08/08/2014–09/05/2014
Nagqu	3.02	260	10	07/15/2014–09/13/2014
Nyainrong	2	0	10	07/10/2014–09/01/2014
Wenjiang	5.25	0	10	07/01/2014–08/07/2014
				09/01/2014–09/07/2014

	Slow Response Measurements (Including Atmospheric Gradient, Soil, and Radiation Observation)[b]			
Site Location	Soil Temperature and Moisture Depths (cm)	Soil Heat Flux Depths (cm)	Gradient Observation Heights (m)	Dates of Data Used
Amdo	5,10,20,40,80,160	5,10	1.5,3,6,12	07/15/2014–09/06/2014
Seng-ge Kambab	4,10,20,60,100	5,5,10	1,2,4,8,18	07/01/2014–09/15/2014
Baingoin	5,10,20,40,100	5,10	2,4,10	07/12/2014–09/03/2014
Biru	5,10,20,40,100	5,10	2,4,10	07/28/2014–09/14/2014
Dali	4,10,20,60,100	4,4,10,20	2,4,10,20	06/30/2014–09/05/2014
Lhari	5,10,20,40,100	5,10	2,4,10	07/26/2014–09/16/2014
Nyingchi	4,10,20,60,100	4,4,10,20	1.3,4.94,9.95,18	08/04/2014–10/02/2014
Namco	0,10,20,40,80,160	5	1.5,2,4,10,20	07/18/2014–09/16/2014
Nagqu	5,10,20,40,80,160	5,10	0.75,1.5,3,6,12,22	07/15/2014–09/13/2014
Nyainrong	5,10,20,50,100	5,10	2,4,8	07/10/2014–09/01/2014
Wenjiang	4,10,20,60,100	4,4,10,20	1.43,4.8,9.05,18.25	07/01/2014–09/15/2014

[a] Most of the sites used unified sonic anemometer (CSAT3, Campbell Scientific Inc.) and CO_2/H_2O Open-Path Gas Analyzer (LI-7500, Licor, USA) except the Seng-ge Kambab site used sonic anemometer (CSAT3A) and Gas Analyzer (EC150).

[b] The temperature, humidity, and wind instruments were installed on the tower; water and soil temperature sensors were installed at the surface. All the 11 sites measure the radiation balance components (incoming and outgoing shortwave, Si, So, and longwave, Li, Lo radiation). (Seng-ge Kambab, Biru, Lhari, and Nyainrong) measure photosynthetic active radiation.

for studying surface thermodynamic properties, and the observational results can be used as a reference for evaluating the quality of satellite retrievals. Therefore, variations of surface albedo at different locations are analyzed here. Many methods (e.g., the flux profile method, the variation method, and the eddy covariance method) have been used to calculate the aerodynamic transfer coefficients, C_D and C_H; however, the eddy covariance method is regarded as the most credible and accurate method [*Zhang et al*., 2002]. The normalized variance of wind speed, temperature, and humidity is used to estimate turbulent transport characteristics of the planetary boundary layer (PBL). Many previous studies [e.g., *Choi et al*., 2004; *Liu and Hong*, 2000; *Chen et al*., 2002; *Bian et al*., 2003] have focused on the variation of turbulent variance with stability in the surface layer and discussed the applicability of Monin–Obukhov similarity theory under different stability conditions. Turbulence kinetic energy (TKE) is another important variable in the PBL, and the TKE budget equation is key point to understand turbulence generation and dissipation.

2. Observational Data and Methods

The 10 Hz raw data from the sonic anemometers and gas analyzer at the 11 flux observational sites are used to calculate turbulence fluxes, variances, and TKE, as well as the Obukhov length (L). In order to get accurate turbulent statistics, EDDYPRO (version 5.1) software is used for data quality control with the following settings: (1) Sets missing more than 11% of the data are not used, and the flux averaging interval is set to 30 min. (2) A double axis rotation for the sonic anemometer tilt correction [*Tanner and Thurtell*, 1969] is used. (3) The block average method is used for turbulent fluctuations. (4) The Webb, Pearman and Leuning density correction [*Webb et al*., 1980] is used for density effects on flux measurements. (5) High/low frequency spectral corrections are used to compensate for flux losses [*Moncrieff et al*., 1997, 2004]. (6) Nine tests derived from *Vickers and Mahrt* [1997] have been utilized to assess the statistical quality of the raw time series.

3. Land Surface Parameters

3.1. Aerodynamic Roughness Length and Thermal Roughness Length

The aerodynamic roughness length z_{0m} and thermal roughness length z_{0h} are two key surface layer variables in the bulk transfer equations to calculate turbulent fluxes in weather and climate models. Recent studies show that it is necessary to distinguish z_{0m} from z_{0h} [e.g., *Beljaars and Holtslag*, 1991] as they have different physical meanings.

The same method is used to calculate z_{0m} for 11 sites. z_{0m} is usually estimated by a least squares fitting multi-height wind speed measurements from PBL tower data under neutral conditions. However, that method is not used in this paper because of a lack of high quality wind gradient data at some sites. Here z_{0m} is obtained from fast response measurements using Monin-Obukhov similarity theory by the relation

$$\ln z_{0m} = \ln z_m - \psi_m\left(\frac{z_{0m}}{L}, \frac{z_m}{L}\right) - kU/u_*, \tag{1}$$

where

$$u_* = \left[\left(\overline{u'w'}\right)^2 + \left(\overline{v'w'}\right)^2\right]^{1/4}, \tag{2}$$

$$\zeta = \frac{z}{L}, L = \frac{-u_*^3}{k\frac{g}{T}\overline{w'T'}}, \tag{3}$$

where the von Karman constant $k = 0.4$, $g = 9.8\ \mathrm{m\ s^{-2}}$ is the gravitational constant, and the sonic anemometer observation height is z_m. U is the horizontal wind speed at level z_m and u_* is the frictional velocity from equation (2). The stability parameter z/L is defined in equation (3). $\overline{w'T'}$ is the sensible heat flux, and ψ_m is the integrated stability correction term for wind profiles. Following the universal functions in *Högström* [1996] and the mathematical form of the correction terms in *Paulson* [1970], for stable surface layers

$$\psi_m\left(\frac{z_{0m}}{L}, \frac{z_m}{L}\right) = -5.3(z_m - z_{0m})/L, (2 > \zeta > 0), \tag{4}$$

and for unstable surface layers

$$\psi_m\left(\frac{z_{0m}}{L}, \frac{z_m}{L}\right) = 2\ln\left(\frac{1+x}{1+x_0}\right) + 2\ln\left(\frac{1+x^2}{1+x_0^2}\right) - 2\tan^{-1}x + 2\tan^{-1}x_0, (-5 < \zeta < 0), \tag{5}$$

$$x = (1 - 19\,z_m/L)^{1/4}, x_0 = (1 - 19\,z_{0m}/L)^{1/4}. \tag{6}$$

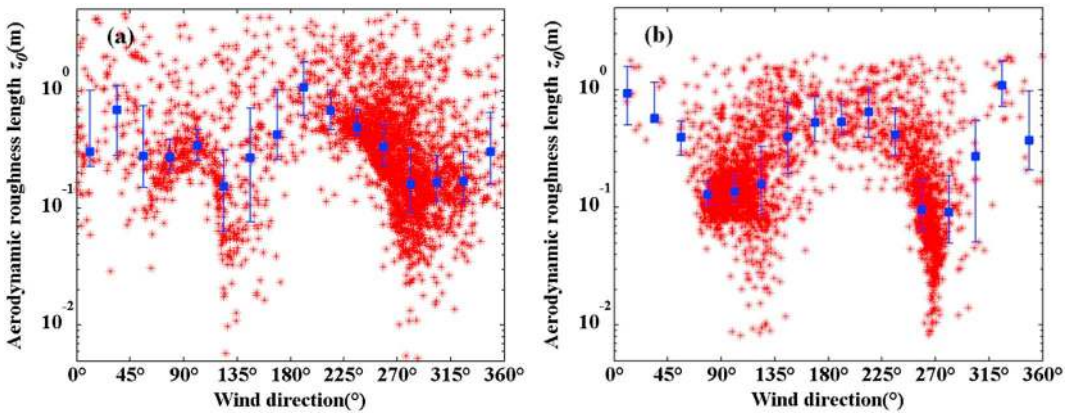

Figure 2. The variation of aerodynamic roughness length z_{0m} for different wind directiona at (a) Seng-ge Kambab and (b) Lhari, respectively.

The temporal variations of z_{0m} are not considered here due to the short 1–2 months period between July and September for each site. However, the heterogeneity of the underlying surface results in vastly different z_{0m} for different wind directions. Figures 2a and 2b show how z_{0m} varies with wind direction at Seng-ge Kambab and Lhari, and z_{0m} from the predominant wind direction (with the largest number of samples) is usually smaller than other wind directions, especially when the wind is obstructed by buildings or mountains near the sites, which are characterized by z_{0m} that is about one or 2 orders of magnitude larger than other land-cover types (e.g., bare soil, alpine steppe, alpine meadow, and cropland). Here we mainly want to obtain a typical z_{0m} value for each site, so obvious buildings or mountains should be excluded. As shown in Figure 3 and Table 3, z_{0m} is mainly determined by land-cover type and canopy height after excluding large obstructions. We see that z_{0m} generally increases in direct proportion to canopy height. z_{0m} at the alpine steppe sites within the small network is an order of magnitude smaller than for cropland or alpine meadow at the eastern sites. In most cases, the median value of z_{0m} within the small network and the east sites are 0.005–0.03 m and 0.1–0.4 m, respectively. The median value of z_{0m} at Amdo is about 0.006 m, which is almost the same as that obtained by *Ma* [2008] over an alpine steppe, and the results at other sites around Amdo about 0.02 m conform well with NPAM (MS3478) site results from the Asia Monsoon Experiment

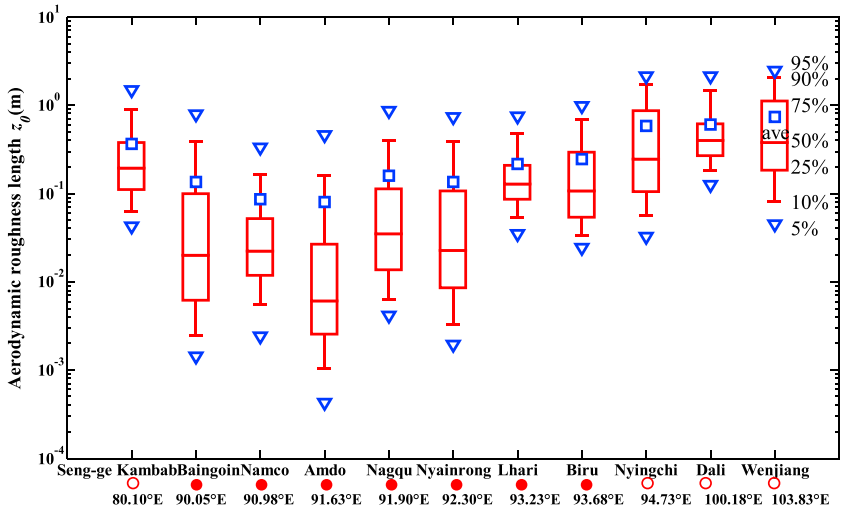

Figure 3. Aerodynamic roughness length (z_{0m}) for each of the 11 sites. The squares represent averaged value. The triangles, error bars, rectangles, and horizontal lines represent 5% and 95%, 10% and 90%, 25% and 75%, and 50% values, respectively. The solid circles represent the sites belonging to the above mentioned small area, and the outlined circles represent the sites far from this area.

Table 3. The Median Value of Aerodynamic Roughness Lengths z_{0m} for the 11 Sites

Sites	Seng-ge Kambab	Baingoin	Namco	Amdo	Nagqu	Nyainrong	Lhari	Biru	Nyingchi	Dali	Wenjiang
z_{0m}	0.196	0.020	0.022	0.006	0.035	0.023	0.135	0.106	0.247	0.399	0.379

on the Tibetan Plateau (GAME/Tibet, 1996-2000). z_{0m} at the Dali and Wenjiang sites over cropland is slightly larger than that obtained for the oasis in the Heihe Basin Field Experiment (HEIFE, 1988–1993) area, owing to few obstructions around the sites.

After z_{0m} has been determined, z_{0h} can be calculated by equation (7) using Monin-Obukhov similarity theory.

$$r_h = \Pr\left[\ln\frac{z_m}{z_{0m}} - \psi_m\left(\frac{z_{0m}}{L},\frac{z_m}{L}\right)\right]\times\left[\ln\frac{z_h}{z_{0h}} - \psi_h\left(\frac{z_{0h}}{L},\frac{z_h}{L}\right)\right]/k^2U, \tag{7}$$

where ψ_h is the integrated stability correction term for temperature profiles [*Högström*, 1996]. For stable surface layers,

$$\psi_h\left(\frac{z_{0h}}{L},\frac{z_h}{L}\right) = -8.0(z_h - z_{0h})/L, (2 > \zeta > 0), \tag{8}$$

and for unstable surface layers,

$$\psi_h\left(\frac{z_{0h}}{L},\frac{z_h}{L}\right) = 2\ln\left(\frac{1+y}{1+y_0}\right), (-5 < \zeta < 0), \tag{9}$$

where

$$y = (1 - 11.6\,z_h/L)^{1/2} \text{ and } y_0 = (1 - 11.6\,z_{0h}/L)^{1/2}. \tag{10}$$

r_h ($\mathrm{m^{-1}\,s}$) is the heat transfer resistance derived from equation (11). H ($\mathrm{W\,m^{-2}}$) is the sensible heat flux, ρ($\mathrm{kg\,m^{-3}}$) is the air density, c_p (=1004 $\mathrm{J\,kg^{-1}\,K^{-1}}$) is the specific heat of air at constant pressure, T is the air temperature at level z_m that is obtained from a linear interpolation between the upper and lower levels, T_g is surface skin temperature derived from equation (12), ULR ($\mathrm{W\,m^{-2}}$) and DLR ($\mathrm{W\,m^{-2}}$) are upward and downward longwave radiation, respectively, and ε is surface emissivity. In order to get relatively accurate results for T_g at different sites, in near-neutral stratification ($-10\,\mathrm{W\,m^{-2}} < H < 10\,\mathrm{W\,m^{-2}}$), set ε to a value that makes the averaged $T_g - T \approx 0$. Here ε need to be set within the range of 0.91 and 0.99 for different sites. Finally, we obtain the excess resistance to heat transfer kB^{-1} from equation (13).

$$H = \rho c_p\frac{T_g - T}{r_h}, \tag{11}$$

$$T_g = \left[\frac{\mathrm{ULR} - (1-\varepsilon)\mathrm{DLR}}{\sigma\varepsilon}\right]^{1/4}, \tag{12}$$

$$kB^{-1} = \ln(z_{0m}/z_{0h}). \tag{13}$$

Many studies have demonstrated that z_{0h} and kB^{-1} are not constant but have obvious diurnal variation [e. g., *Yang et al*., 2007; *Ma et al*., 2008]. The variation of z_{0h} can be described by the change of kB^{-1}, so here we just analyze kB^{-1} for all the sites except for Wenjiang (due to insufficient samples). There exist many factors that influence kB^{-1}, such as meteorological conditions, the structure of the vegetation, surrounding obstructions, radiation, and soil surface resistance. In Figure 4, almost all of the sites show diurnal variation for kB^{-1}, and the diurnal curves of kB^{-1} are approximately parabolic with a maximum at noon and minimum at night. However, the amplitudes of the variation in kB^{-1} for the 10 sites are obviously different. In most cases, especially in daytime kB^{-1} is positive. However, negative values of kB^{-1} are reported at night for smooth surfaces over TP as shown in Figure 4d at the Amdo site. This means that heat transfer efficiency may exceed that of momentum [*Verhoef et al*., 1997; *Yang et al*., 2007]. Rough surfaces usually have larger kB^{-1} than smooth surfaces, mainly because rough surfaces affect z_{0m} more than z_{0h}. Consequently, kB^{-1} generally increases with z_{0m}. In comparison with kB^{-1}, for the sites within the "small network" in the middle of the TP with alpine steppe, the median kB^{-1} is in the range of 1.67 to 3.86, while kB^{-1} at other sites with larger z_{0m} is in the range of 2.29 to 7.38, as shown in Table 4. Note, kB^{-1} at Seng-ge Kambab with bare soil is obviously larger than

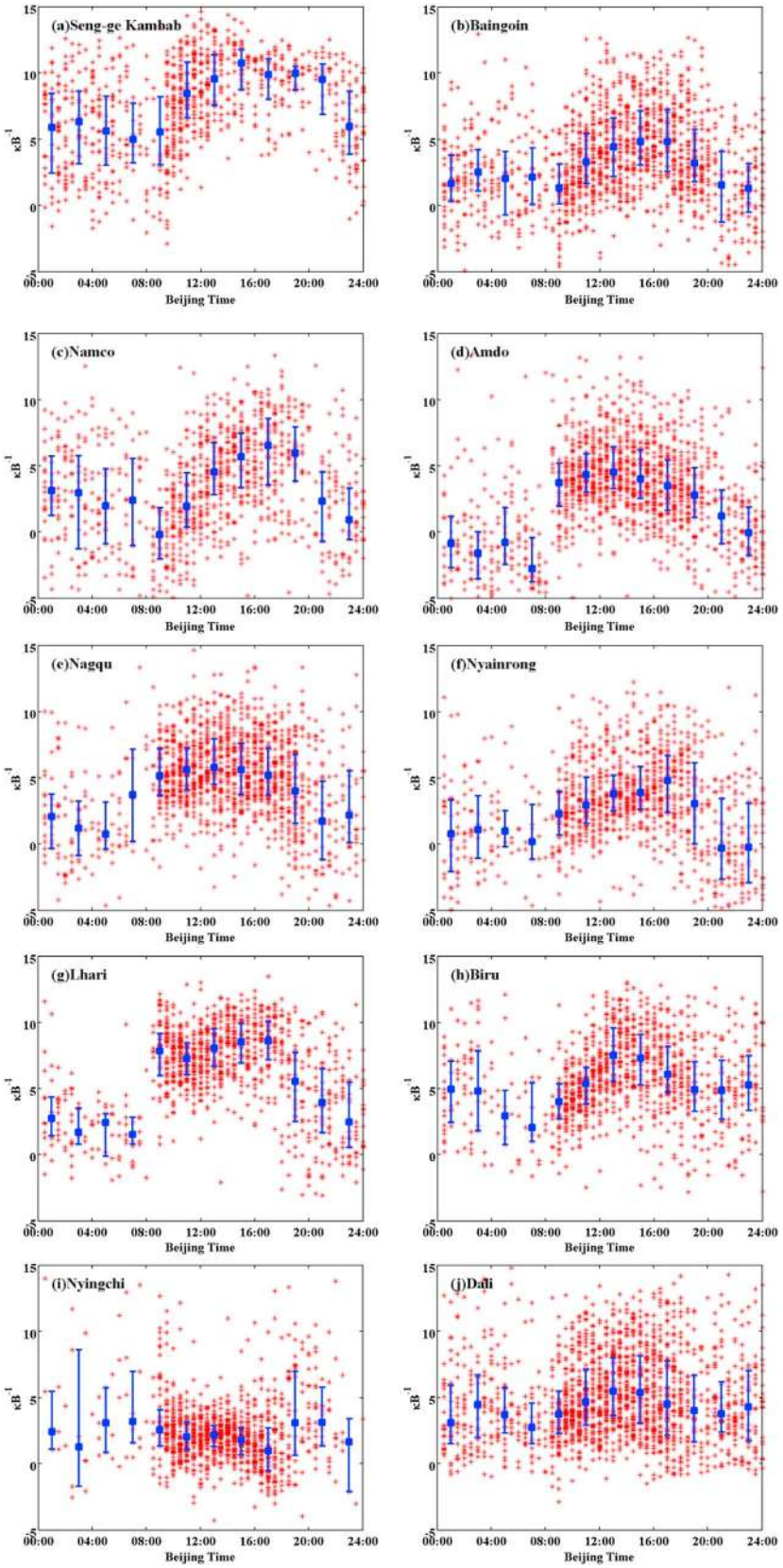

Figure 4. kB^{-1} values derived from observed heat fluxes, temperature, and wind speed for the 10 sites. (a) Seng-ge Kambab, (b) Baingoin, (c) Namco, (d) Amdo, (e) Nagqu, (f) Nyainrong, (g) Lhari, (h) Biru, (i) Nyingchi, and (j) Dali.

Table 4. Median Values of kB^{-1} for the 10 Sites

Sites	Seng-ge Kambab	Baingoin	Namco	Amdo	Nagqu	Nyainrong	Lhari	Biru	Nyingchi	Dali
kB^{-1}	7.38	2.34	2.67	1.98	3.86	1.67	4.73	4.94	2.29	4.14

some published results [*Kohsiek et al*., 1993; *Voogt and Grimmond*, 2000] due to the rougher surface. It is worthwhile to note that kB^{-1} at Nyingchi is almost constant during daytime, and some studies [e.g., *Verhoef et al*., 1997] have found this also over savannah. Meanwhile, kB^{-1} at Nyingchi is uncertain at night as a result of a near zero heat flux.

3.2. Albedo (α)

Surface albedo α is defined as the ratio of the total downward solar radiation at the land surface S_d to the total upward solar radiation S_u:

$$\alpha = \frac{S_u}{S_d}. \tag{14}$$

Surface albedo is important for studying the surface thermodynamic properties. The diurnal variation of α varies at different sites, since α is affected by many factors (e.g., weather conditions, solar elevation, soil moisture, and vegetation cover). Figures 5a and 5b show the average surface albedo for the 11 sites during the observation period. The surface albedo over the midwestern TP is usually larger than that over the eastern and southeastern TP. The surface albedo at Seng-ge Kambab with bare soil is about 0.211, which is smaller than QXPMEX [*Zhang et al*., 1988]. Other research shows that the MODIS-derived albedo meets the absolute accuracy of 0.02 as required by climate models in a semidesert region on the Tibetan Plateau [*Wang et al*., 2004]. The MODIS-derived albedo results are essentially in agreement with ground measurements. The surface albedo of the alpine meadow sites ranges from 0.151(Namco) to 0.219 (Amdo). In general, our results are slightly smaller than the QXPMEX results. One of the reasons may be the difference in averaging period in our study, which was mainly from July to September, while QXPMEX results are averaged values from May to September. The wet season usually arrives from late May to late June over TP, and damp soil during the wet season decreases the surface albedo. Table 5 shows the correlation between daily mean value of surface albedo and soil moisture at the 11 sites during the wet season. We find that α is significantly negatively correlated with soil moisture for dry soils and sparse vegetation. However, there is no significant negative correlation for thick vegetation and moist soils in most cases. Many studies have shown that surface albedo has an exponential relation with soil moisture [*Liu et al*., 2008; *David and Asner*, 2002]. According to the fitted exponential equation, when soil moisture is less than 0.2 $m^3\,m^{-3}$, α decreases rapidly with increasing soil moisture. However, the relation between them remains fairly constant when soil moisture is larger than 0.2 $m^3\,m^{-3}$, and larger scatter also appears [*Liu et al*., 2008]. Meanwhile, because of the small number of samples (about 50), relatively insignificant small positive or negative correlations coexist for the sites with moist soils.

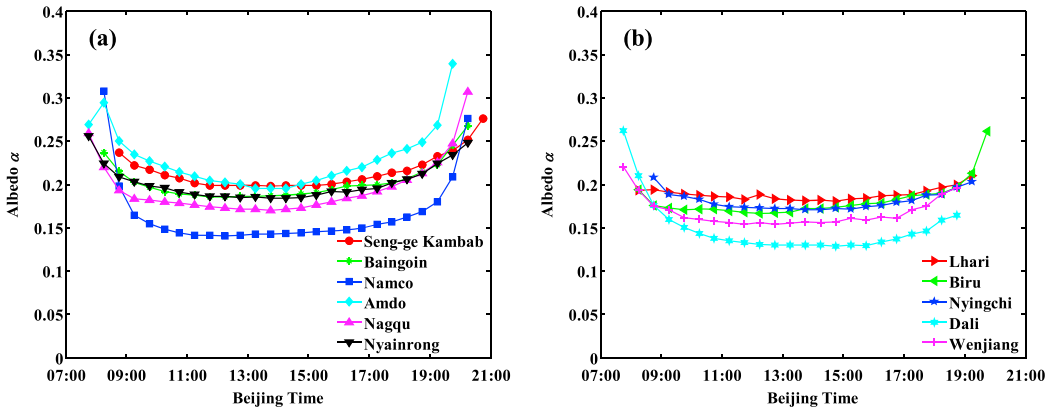

Figure 5. The diurnal variations of surface albedo (α) for the 11 sites.

Table 5. Daily Mean Surface Albedo (α), Daily Mean Soil Moisture (W_s), and the Correlation Coefficient (R) Between Them (N is the Number of Samples)

Sites	Seng-ge Kambab	Baingoin	Namco	Amdo	Nagqu	Nyainrong	Lhari	Biru	Nyingchi	Dali	Wenjiang
α	0.211	0.196	0.151	0.219	0.183	0.195	0.187	0.176	0.178	0.140	0.161
W_s	0.052	0.152	0.113	0.324	0.241	0.283	0.461	0.406	0.320	0.404	0.376
$R(N)$	−0.74 (77)	−0.851 (54)	−0.817 (50)	−0.169 (54)	−0.309 (59)	0.469 (54)	0.416 (53)	0.093 (49)	0.088 (58)	−0.622 (68)	0.111 (41)

Surface albedo at all the sites decreases with solar elevation with a typically parabolic curve and minimum values at around 1200 local time. Sunny and partly cloudy conditions predominate over the midwestern TP at higher elevations, but the eastern TP and Chengdu plain usually have greater cloud amount. Therefore, the range of diurnal variation at the midwestern TP is larger than at the eastern TP and Chengdu plain.

4. The Turbulence Characteristics of the Surface Layer Over the Tibetan Plateau and Surrounding Region

4.1. Bulk Transfer Coefficients for Momentum (C_D) and Heat (C_H)

In the surface layer, bulk transfer equations can be written as

$$C_D = \frac{u_*^2}{U_{10m}^2}, \tag{15}$$

$$C_H = \frac{\overline{w'T'}}{U_{10m}(T_g - T_{2m})}. \tag{16}$$

Here C_D and C_H are at a standard 10 m for convenience in comparing the sites. U_{10m} (m s^{-1}) and T_{2m} (K) are the mean wind speed at 10 m and air temperature at 2 m, respectively. If the sites do not have observations at 10 m or 2 m, we use linear interpolation to obtain the values.

The first and second Tibetan Plateau Atmospheric Scientific Experiment (TIPEX I and II) results showed that C_D at the midwestern TP is smaller than that at the eastern TP. As shown in Figure 6 and Table 6, at the eastern and southeastern side of the TP, C_D values are 8.0×10^{-3} – 12.6×10^{-3}, but in the middle of the TP within the "small network" C_D values are 2.9×10^{-3} – 4.4×10^{-3} over the alpine steppe without obstructions. The average values of C_D at Seng-ge Kambab, Lhari, and Biru are about 10.0×10^{-3}; these are significantly larger than the theoretical value of bare soil and alpine steppe due to obstructions and mountain effects. The differences in C_H between sites are smaller than for C_D, in the western part of the TP C_H is 2.4×10^{-3}, in the middle of the TP within the "small network" C_H values are 2.2×10^{-3} – 3.8×10^{-3}, and in the eastern and southeastern side of TP C_H values are 3.4×10^{-3} – 6.0×10^{-3}. Our results for C_D and C_H over mideastern TP are in good agreement with the Qamdo site [*Bian et al.*, 2002] over the alpine steppe during TIPEXII. The other two sites in TIPEX II, Gerze [*Liu and Hong*, 2000] and Damxung [*Chen et al.*, 2002], over the western TP with a smoother surface have smaller C_D and C_H relative to the eastern sites. Whether C_D is smaller or larger than C_H has been controversial for a long time. In this study, $C_D \geq C_H$ in most cases. However, some studies have suggested that $C_D < C_H$. According to our results, different calculation methods may be the main reason for the opposite conclusion rather than surface properties at the different sites. The flux profile method usually leads to $C_D < C_H$ [*Ma*, 1990; *Li et al.*, 2002], while the eddy correlation method results in $C_D \geq C_H$ [*Feng et al.*, 2011; *Liu and Hong*, 2000]. Furthermore, both C_D and C_H increases with z_{0m}, but C_D increases faster than C_H. *Mahrt* [1996] and *Yang et al.* [2007] speculated that form drag contributes significantly to C_D but contributes less to heat transfer.

For unstable stratification, the atmospheric turbulent motion is mainly thermal turbulence when the wind speed is low so that the upper part of the surface layer is in the local free convection regime. This condition often leads to larger bulk transfer coefficients for C_D and C_H. Shear production of turbulence increases with wind speed, and both C_D and C_H decrease rapidly with wind speed. As shown in Figure 7, when the wind speed exceeds a certain threshold (about 6 m s^{-1} at Amdo), both C_D and C_H vary little with wind speed. For stable stratification, both C_D and C_H increase with wind speed at low wind speeds. The stratification in the surface layer becomes approximately neutral as wind speed increases. The increased wind shear

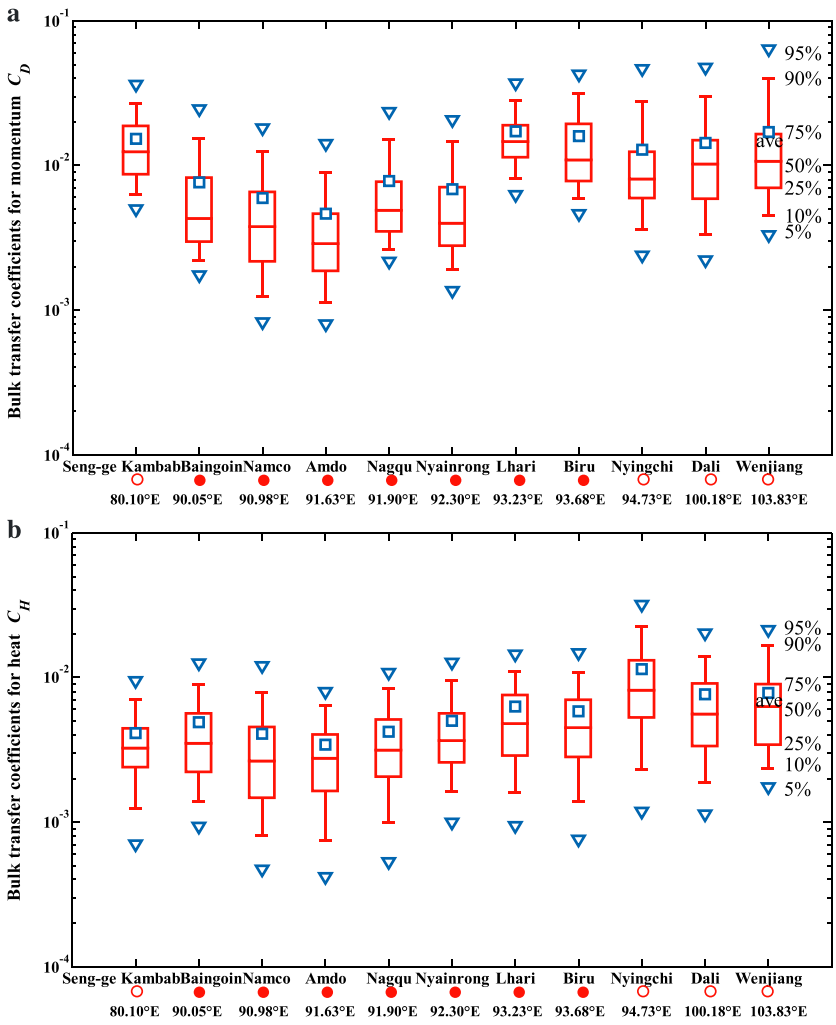

Figure 6. (a) Bulk transfer coefficients for momentum (C_D) and (b) bulk transfer coefficients for heat (C_H) for the 11 sites. The squares represent the averaged value. The triangle, error bar, rectangle, and straight line represent 5% and 95%, 10% and 90%, 25% and 75%, and 50% values, respectively. Solid circles denote the sites belonging to the small area, and outlined circles denote the sites that are far from this area.

generates more mechanical turbulence which weakens the temperature inversion. The relationship between wind speed and C_D or C_H is consistent with a power law relation for unstable stratification. However, the functional form is uncertain for stable stratification.

As shown in Figure 8, it was once thought that C_D increases monotonically with increasing instability as predicted by Monin-Obukhov similarity. However, *Srivastava and Sharan* [2015] found that the variation of C_D with z/L over a tropical environment in unstable conditions is bounded. The curve first shows an increase with z/L until it reaches a peak for weakly unstable conditions ($z/L \approx -0.12$) and then decreases with increasing instability. For the 11 sites here, C_D increases monotonically with increasing instability from stable conditions to weakly unstable conditions, but C_D does not significantly change with increasing instability from weakly unstable to strongly unstable. Namco, Biru, and Nyingchi even show the same behavior observed by *Srivastava and*

Table 6. The Median Value of the Bulk Transfer Coefficients for the 11 Sites Under Neutral Conditions

Sites	Seng-ge Kambab	Baingoin	Namco	Amdo	Nagqu	Nyainrong	Lhari	Biru	Nyingchi	Dali	Wenjiang
C_D	0.0096	0.0034	0.0038	0.0029	0.0044	0.0038	0.0105	0.0101	0.0080	0.0116	0.0126
C_H	0.0024	0.0027	0.0022	0.0024	0.0028	0.0032	0.0038	0.0034	0.0060	0.0045	0.0047

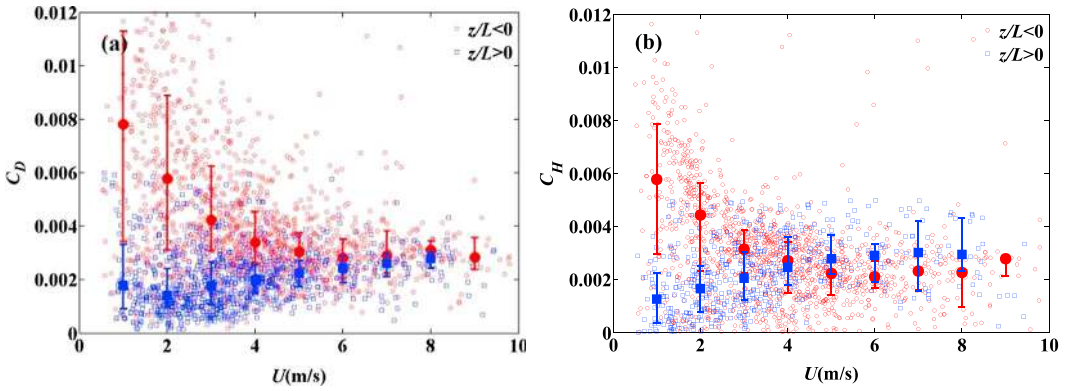

Figure 7. Relationship between (a) bulk transfer coefficients for momentum (C_D), (b) bulk transfer coefficients for heat (C_H), and wind speed at Amdo. The red circles and blue squares represent median value for unstable and stable condition, respectively. The error bars represent 25% and 75% probability values.

Sharan [2015] (figure omitted), i.e., C_D decreasing with increasing instability from weakly unstable to strongly unstable. In contrast, the relationship between C_H and z/L seems relatively straightforward; C_H increases monotonically with increasing instability at all the sites.

4.2. Turbulent Variances

The variation of turbulent variance with z/L has attracted the attention of many researchers over the years. Monin-Obukhov similarity theory predicts that in the surface layer any turbulent variance (σ_x) normalized by the scaling parameter $x_*\left(\equiv\overline{w'x'_0}/u_*\right)$ is a normalized function of z/L [*Andreas et al.*, 1998; *Choi et al.*, 2004]:

$$\sigma_x/x_* = \phi_x(z/L) = C_{x1}(1 - C_{x2}z/L)^{\pm 1/3}, \tag{17}$$

where σ_x is the standard deviation of x, and x denotes the three wind components, temperature, or humidity, ϕ_x is the normalized stability function, and C_{x1} and C_{x2} are empirical constants. Positive (negative) sign for the exponent corresponds to wind components (scalars).

As $-z/L \to \infty$ the surface layer approaches local free convection and, equation (17) becomes

$$\sigma_x/x_* = \phi_x(z/L) = C_x(-z/L)^{\pm 1/3}, \tag{18}$$

where $C_x = C_{x1}C_{x2}^{\pm 1/3}$ is a similarity constant.

As shown in Figure 9 and Table 7, the variance of the wind components follow the one-third power of normalized height for all 11 sites for unstable conditions. (Figures for the sites except Amdo are omitted.) For the neutral condition, $C_{u1} \approx C_{v1} > C_{w1}$. It is well known that the scatter in the horizontal direction is larger than that in the vertical direction. Turbulence in the vertical direction is subject to thermal forcing, but not in the

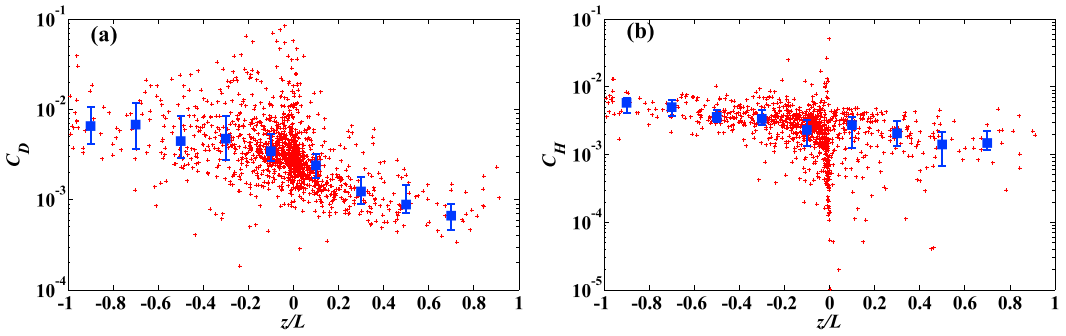

Figure 8. Relationship between (a) bulk transfer coefficients for momentum (C_D), (b) bulk transfer coefficients for heat (C_H), and stability (z/L) at Amdo. The squares represent median value. The error bar represent 25% and 75% probability values, respectively.

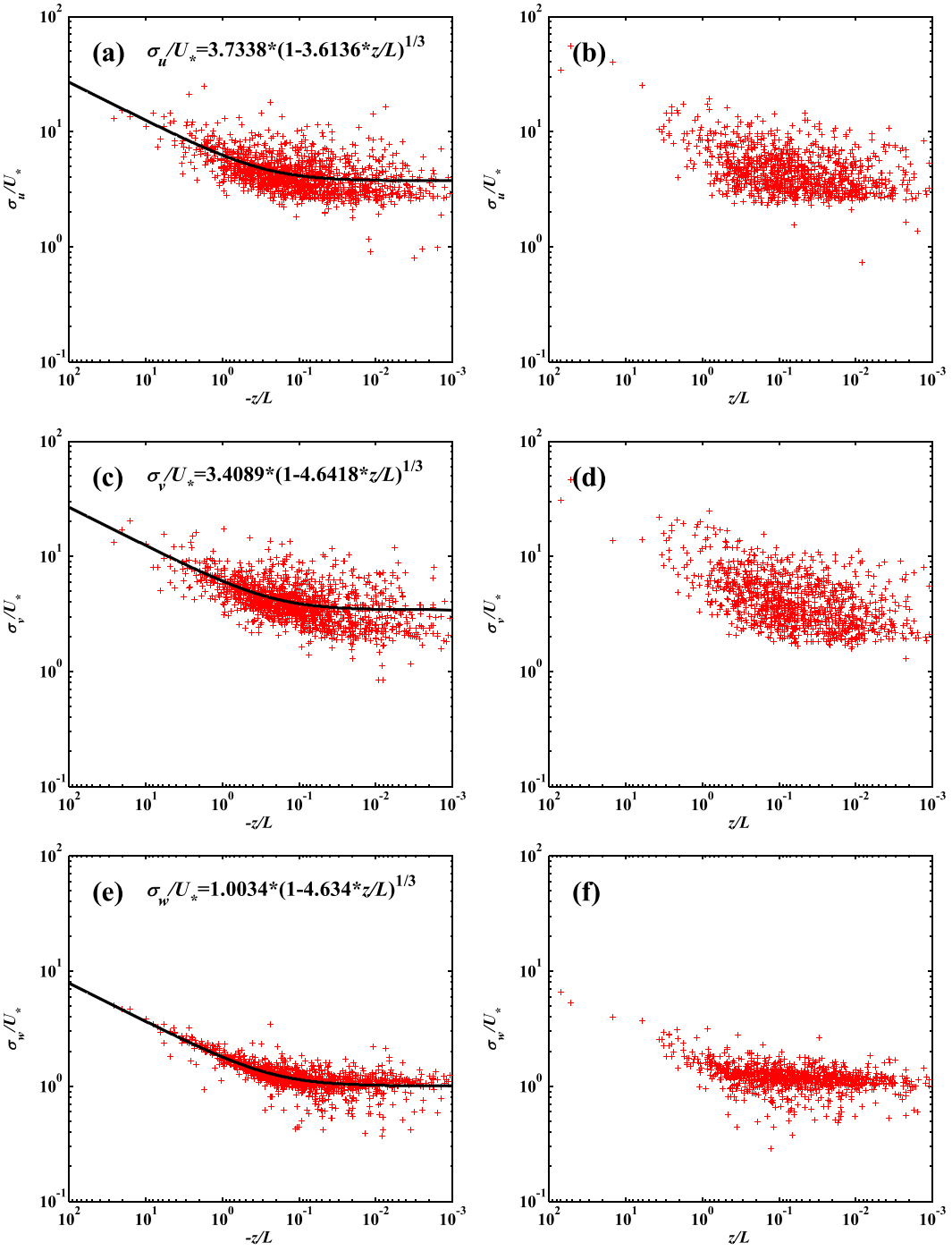

Figure 9. The relationship between normalized standard deviations of (a, b) horizontal wind component, *u*, (c, d) horizontal wind component, *v*, and (e, f) vertical wind *w* with stability *z*/*L*. Solid lines are the fitted normalized functions for σ_u/u_*, σ_v/u_*, and σ_w/u_* under unstable stratification ($z/L < 0$) at Amdo.

horizontal direction. Compared with the result from fitting curves over the TP, ($\sigma_u/u_*, \sigma_v/u_*, \sigma_w/u_*$) for neutral conditions at Wenjiang (Chengdu plain) is significantly less than elsewhere on the TP and surrounding region sites. However, σ_w/u_* for TP and plain sites are almost the same. *Zhao* [1991] pointed out that horizontal direction disturbance results from "large" quasi-horizontal turbulence that "remembers" upwind terrain features. The quasi-horizontal turbulence may produce larger variances relative to the local surface stress and that may be the main reason for the larger scatter in horizontal wind speed variances. For stable stratification

Table 7. Wind Speed Variance Normalized by Characteristic Scale Parameters for Neutral Stratification (C_{u1}, C_{v1}, C_{w1}), Temperature, and Humidity Variance Normalized by a Characteristic Scale Parameter for Free Convection ($z/L < -0.1$) (C_T, C_q)

Site Location	C_{u1}	C_{v1}	C_{w1}	C_T	C_q
Amdo	3.73	3.41	1.00	1.27	2.43
Seng-ge Kambab	2.64	2.66	1.18	0.95	3.60
Baingoin	3.84	3.50	0.95	1.17	1.74
Biru	3.21	2.89	0.85	1.10	2.17
Dali	2.49	2.22	1.05	1.18	2.40
Lhari	3.41	2.62	1.25	1.08	1.86
Nyingchi	3.22	2.90	1.18	1.06	2.62
Namco	2.87	2.94	1.12	1.10	2.22
Nagqu	3.61	3.14	1.04	1.24	1.76
Nyainrong	3.77	3.57	0.95	1.18	1.61
Wenjiang	2.05	1.98	0.98	1.30	2.03
Gerze	3.21	2.69	1.46	1.45	2.96
Damxung	3.40	2.45	1.15	1.25	1.27
Qamdo	3.45	3.15	1.30	1.00	5.30
Rongbuk Valley	3.10	2.93	1.05	1.15	1.54

($z/L > 0$), the scatter of C_x is larger, high frequency fluctuations are restrained with increasing stability z/L. For $0 < z/L < 0.1$, the surface layer is approximate neutrally stratified and C_x is basically a constant. For strong stable stratification ($z/L > 0.1$), intermittent turbulence and gravity waves play a major role.

As shown in Figure 10, the measured $\sigma_T/|T_*|$ and $\sigma_q/|q_*|$ follow well Monin-Obukhov theory for strongly unstable stratification ($z/L < -0.1$) at Amdo. In this regime, the temperature variance normalized by the temperature scale C_T is in the range of 0.95 to 1.45 for the 11 sites. Previous research results for Garze [*Liu and Hong*, 2000], Damxung [*Chen et al*., 2002], Qamdu [*Bian et al*., 2003], and Rongbuk Valley [*Liu and Feng*, 2007] indicate that C_T is the same at different sites. The scatter of C_T is larger relative to C_{w1}. For stable stratification ($z/L > 0$), larger scatter appeared with no obvious universal functional relations. However, C_T usually decreases with stability z/L, and C_T is almost constant for strong stable stratification. Because accurate measurement of small heat flux is difficult for near-neutral stratification, larger scatter is often evident; nonstationarity may be another reason for larger scatter. The range of the humidity variance normalized by the humidity scale C_q is in the range of 1.27 to 5.3. C_q tends to be larger than C_T with unpredictable differences among different regions. Many previous studies [e.g., *Katul and Hsieh*, 1999] have also found this, suggesting a dissimilarity between heat and water vapor transfer, which is supported by our study.

The stable stratification regime ($z/L > 0$) is often divided into two parts [e.g., *Derbyshire*, 1990; *Malhi*, 1995]: weakly stable conditions and strongly stable conditions (characterized by intermittent turbulence). As shown in Figure 11, the relationship between $\overline{w'T'}$ and z/L is V shaped, and $\overline{w'T'}$ reaches a minimum at $z/L \approx 0.07$. For weakly unstable conditions ($0 < z/L < 0.07$), turbulence is well described by similarity theory, and $\overline{w'T'}$ decreases rapidly with increasing z/L. For strongly stable conditions ($z/L > 0.07$), motions such as intermittent turbulence and waves occur, and $\overline{w'T'}$ increases with increasing z/L; the development of these kinds of motion seems to facilitate scalar turbulent transport. The critical value (z'/L) of the stability, at which the minimum in $\overline{w'T'}$ occurs, varies for different surface properties, and is typically in the range of 0.06 to 0.2 [*Malhi*, 1995; *Mahrt*, 1996; *Zhou et al*., 2005], presumably due to differing thermodynamic and dynamic characteristics for different places. Table 8 shows the results for the 11 sites; most of the z'/L values at the TP sites are centered around 0.04, which is smaller than that at plains sites.

4.3. TKE and Components in TKE Equation

The shear $\left(-\partial\overline{u}/\partial z\overline{u'w'} - \partial\overline{v}/\partial z\overline{v'w'}\right)$ and buoyancy terms $\left(g/T\overline{w'T'}\right)$ in the TKE equation maintain the turbulent motions. In order to simplify calculations, the x axis is directed along the average wind. Assuming horizontal homogeneity and no mean divergence, the TKE equation is written as

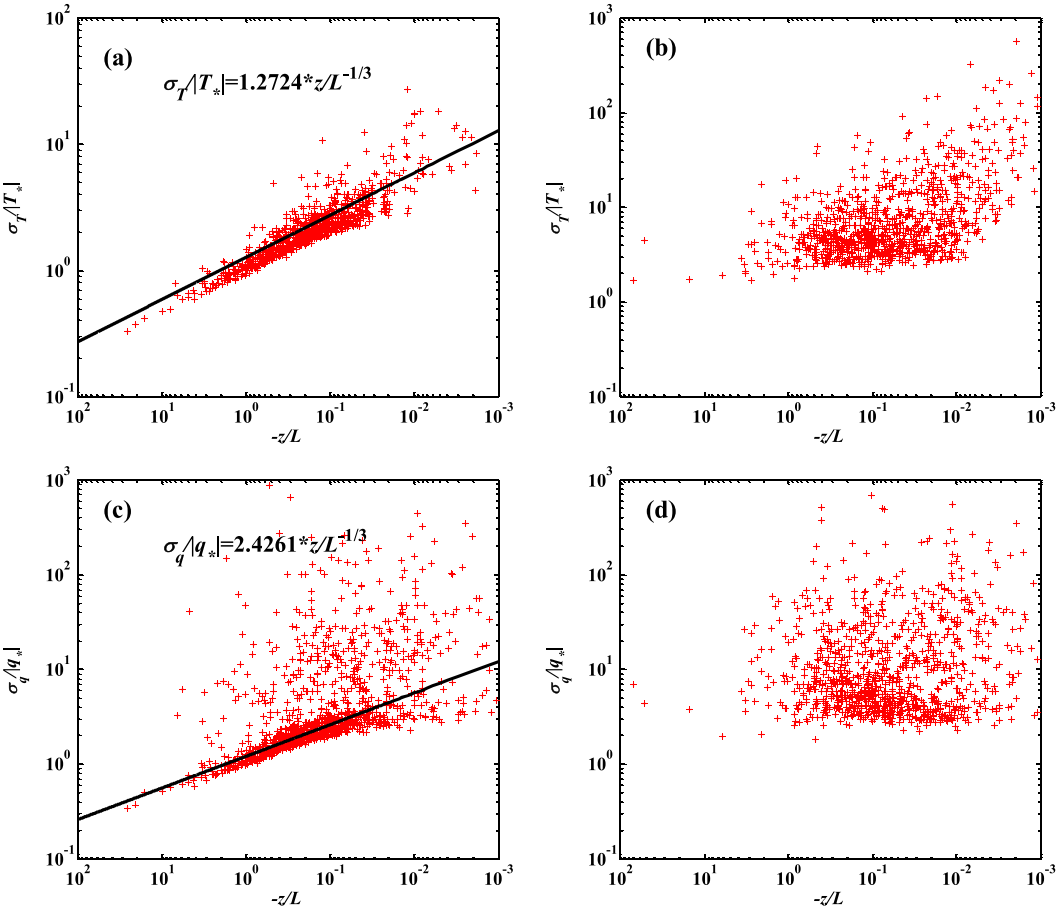

Figure 10. The relationship between normalized standard deviations of (a)--(b) temperature and (c)--(d) humidity with stability z/L. Solid lines are the fitted normalized functions for $\sigma_T/|T_*|$ and $\sigma_q/|q_*|$ for free convection ($z/L < -0.1$) at Amdo.

$$\frac{\partial \bar{e}}{\partial t} = \frac{g}{T}\overline{w'T'} - \overline{u'w'}\frac{\partial \bar{u}}{\partial z} - \frac{\partial\left(\overline{w'e}\right)}{\partial z} - \frac{1}{\bar{\rho}}\frac{\partial\left(\overline{w'p'}\right)}{\partial z} - \varepsilon. \tag{19}$$

The left side of equation (19) is the local time variation $\partial\bar{e}/\partial t$, and the terms on the right-hand side of equation (22) describe the buoyancy and shear energy production or consumption, turbulent transport of $\bar{e}$, pressure correlation, and viscous dissipation [*Stull*, 1988]. The eddy correlation method is used to calculate $\overline{w'T'}$, $\overline{u'w'}$ and $\bar{e} = 1/2\left(\overline{u'^2 + v'^2 + w'^2}\right)$, and $\partial\bar{u}/\partial z$ in the surface layer is estimated as

$$\frac{\partial \bar{u}}{\partial z} = \phi_m(\zeta)\frac{u_*}{kz}, \tag{20}$$

where the nondimensional wind profiles ϕ_m [*Högström*, 1996] is

$$\phi_m(\zeta) = 1 + 5.3\, z_m/L, (2 > \zeta > 0), \tag{21}$$

$$\phi_m(\zeta) = (1 - 19\, z_m/L)^{-1/4}, (-5 < \zeta < 0). \tag{22}$$

Since $\partial\bar{u}/\partial z > 0$ and $-\overline{u'w'} > 0$, the shear term $-\partial\bar{u}/\partial z\overline{u'w'} > 0$.

The variation of $\bar{e}$ for different stratification in surface layer is controlled by both the shear and buoyancy term. For stable stratification, the buoyancy term is usually small and negative; the shear term becomes almost the only source of $\bar{e}$. Therefore, $\bar{e}$ is much smaller for stable stratification than for neutral or unstable stratification. For unstable stratification, the buoyancy term in the surface layer is large and positive due to thermal instability; both shear and buoyancy terms made an important contribution to $\bar{e}$ except the case

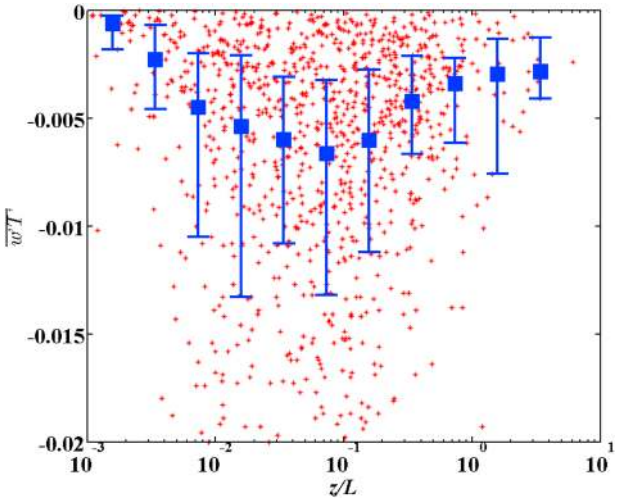

Figure 11. Relationship between heat flux $\left(\overline{w'T'}\right)$ and stability (z/L) at Amdo. The squares denote median values. The error bars represent 25% and 75% probability values, respectively.

for zero or very light wind. As shown in Figures 12a and 12b, the shear term has a significant positive correlation with $\bar{e}$ under both unstable and stable stratification; the relationship between them follows a power function relationship. However, buoyancy term has a significant positive correlation with $\bar{e}$ only under unstable stratification; insignificant correlations exist under stable stratification. The above conclusion about the relationship between shear and buoyancy terms with $\bar{e}$ is basically in agreement with the results at Dingxi over the Loess Plateau in Northwest China [*Yue et al.*, 2015]. Figures 13a–13c show that the shear and buoyancy terms as well as $\bar{e}$ over the TP are larger than over the southeastern TP and Wenjiang (Chengdu plain). For unstable stratification, the buoyancy term generally decreases from west to east; this trend still exists within the "small network," which is the main reason for the similar trend in $\bar{e}$. The greatest wind shear production occurs in the surface layer due to large $\partial\bar{u}/\partial z$. Because the wind speed gradually decreases from the western to the southeastern TP and adjacent plain, the shear term also generally decreases from west to east, but Lhari and Biru are obvious exceptions; there is no obvious trend within the "small network." The variations of $-\overline{u'w'}$ at the different sites play a major role in the differences for shear term within the "small network." $\bar{e}$ in neutral stratification sometimes can exceed the value for unstable stratification due to a larger shear term at some sites. Overall, larger shear and buoyancy terms over the TP can produce larger $\bar{e}$ relative to the low elevation regions especially in unstable and neutral stratification.

4.4. Turbulent Fluxes

We use the eddy covariance method to calculate turbulent fluxes of momentum (τ), sensible heat (H), and latent heat (LE):

$$\tau = \rho u_*^2, \tag{23}$$

$$H = \rho c_p \overline{w'T'}, \tag{24}$$

$$LE = L_v \overline{w'\rho_v'}. \tag{25}$$

As shown in Figures 14a and 14b, τ has obvious diurnal variation at all the sites. In general, τ is usually small during the night and increases after sunrise, with a morning minimum and a maximum around 1500 local time. In most cases, τ in the midsection of the TP is larger than that over the southeastern part of the TP and Wenjiang (Chengdu plain). The main reasons are wind speed and z_{0m} variations for 11 sites. Figures 14g and 14h show the diurnal variation of 10 m wind speed for the 11 sites. Stronger wind speed in the midsection of the TP causes larger momentum flux relative to the southeastern TP and plain region. As Figures 14a and 14b and 14g and 14h show the amplitude and time of maximum and minimum values of τ correspond to those of wind speed. Figures 15a and 15d also show that the daily variations of τ and wind speed are significantly correlated. τ obviously increases during strong wind periods (e.g., from July 23 to July 25 and from August 24 to August 26 for the "small network" sites). On the other hand, the same wind speed

Table 8. The Minimum $\overline{w'T'}$ Corresponding z/L (z'/L) for the 11 Sites

Sites	Seng-ge Kambab	Baingoin	Namco	Amdo	Nagqu	Nyainrong	Lhari	Biru	Nyingchi	Dali	Wenjiang
z'/L	0.04	0.03	0.02	0.07	0.10	0.04	0.02	0.02	0.08	0.03	0.15

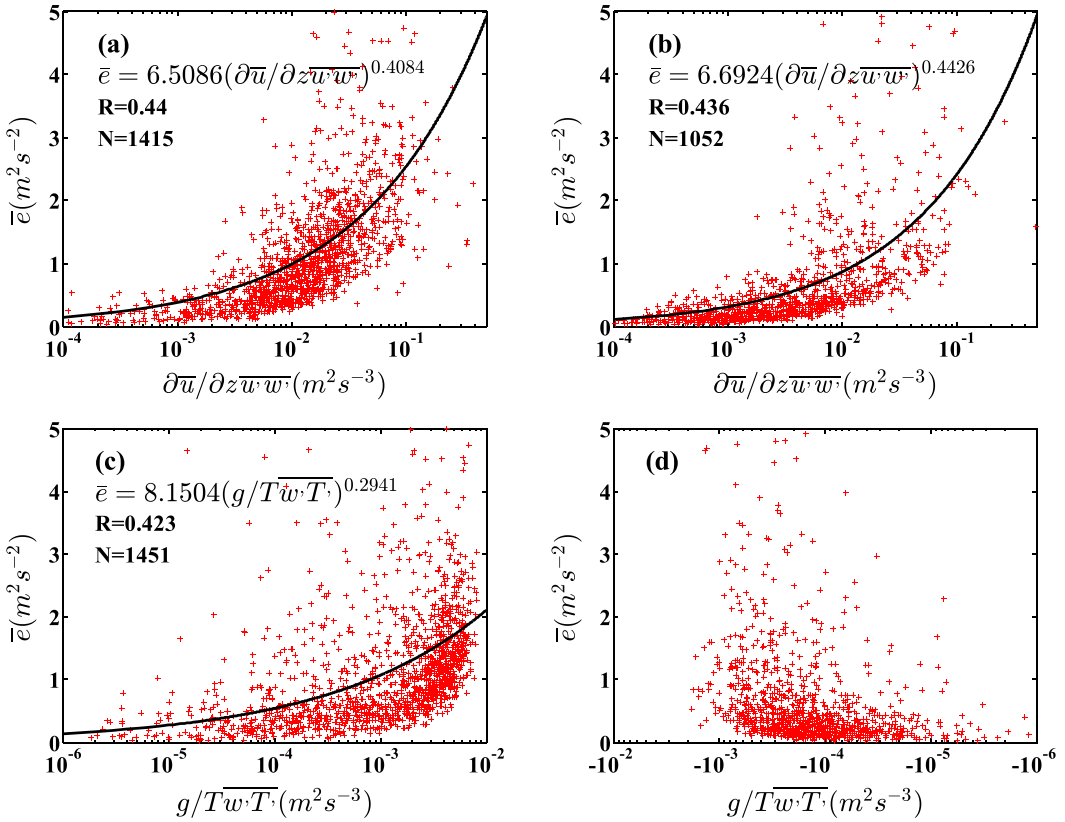

Figure 12. The relationship between (a, b) the shear term $\left(-\partial\overline{u}/\partial z\overline{u'w'}\right)$ and (c, d) the buoyancy term $\left(g/T\overline{w'T'}\right)$ with $\bar{e}$ at Amdo. Solid lines are the fitted functions; *N* represents the number of samples and *R* represents the correlation coefficient.

can produce more turbulence over a rough surface compared to a smooth surface. Despite the wind speed at Seng-ge Kambab and other sites over the TP being same strength in the afternoon under unstable conditions, τ at Seng-ge Kambab is obviously larger than other sites. Although wind speed at Namco is about twice that of the other sites on the TP at night, τ at Namco is only slightly larger than other sites. The combined action of wind speed and underlying surface roughness determines the momentum flux difference between different sites.

Figures 14c and 14d show the diurnal variation of *H*. Overall, *H* gradually decreases from west to east. The diurnal variation usually peaks at about 1300 LT at all 11 sites. The maximum is close to 200 W m^{-2} over the western TP (Seng-ge Kambab), while it is less than 70 W m^{-2} over the Chengdu plain (Wenjiang). The maximum is about 130 W m^{-2} at Namco, but there seems to be little difference between the other sites within the "small network" whose maximums are about 75 W m^{-2}. Sensible heat flux at Nyingchi and Dali seems to be slightly larger than the results within the "small network."

As shown in Figures 13e and 13f, the spatial distribution of *LE* is different from and more complicated than *H*. The diurnal maximum and minimum also occur at same local time as *H*. The diurnal variation peak is only about 20 W m^{-2} over western TP (Seng-ge Kambab). However, *LE* does not simply increase from west to east. For the sites within the "small network," the maxima of *LE* can approach 250 W m^{-2} at the sites near 32°N over mideastern TP, and other sites at 29.5°N to ~31.5°N in the south are slightly smaller than the sites to the north. Dali cropland on the southeastern side of the TP has the largest *LE* among the 11 sites; the maximum can exceed 250 W m^{-2}. *LE* on the Chengdu plain (Wenjiang) is the same as that of the sites on the same latitude over the mideastern TP.

The daytime variations of *H* and *LE* mainly result from (1) the energy available from the difference between the net radiation R_n and soil heat flux G_0. In contrast with R_n, G_0 is usually relatively small. R_n is mainly effected by the attenuation of solar radiation by clouds at the top of the atmosphere as a

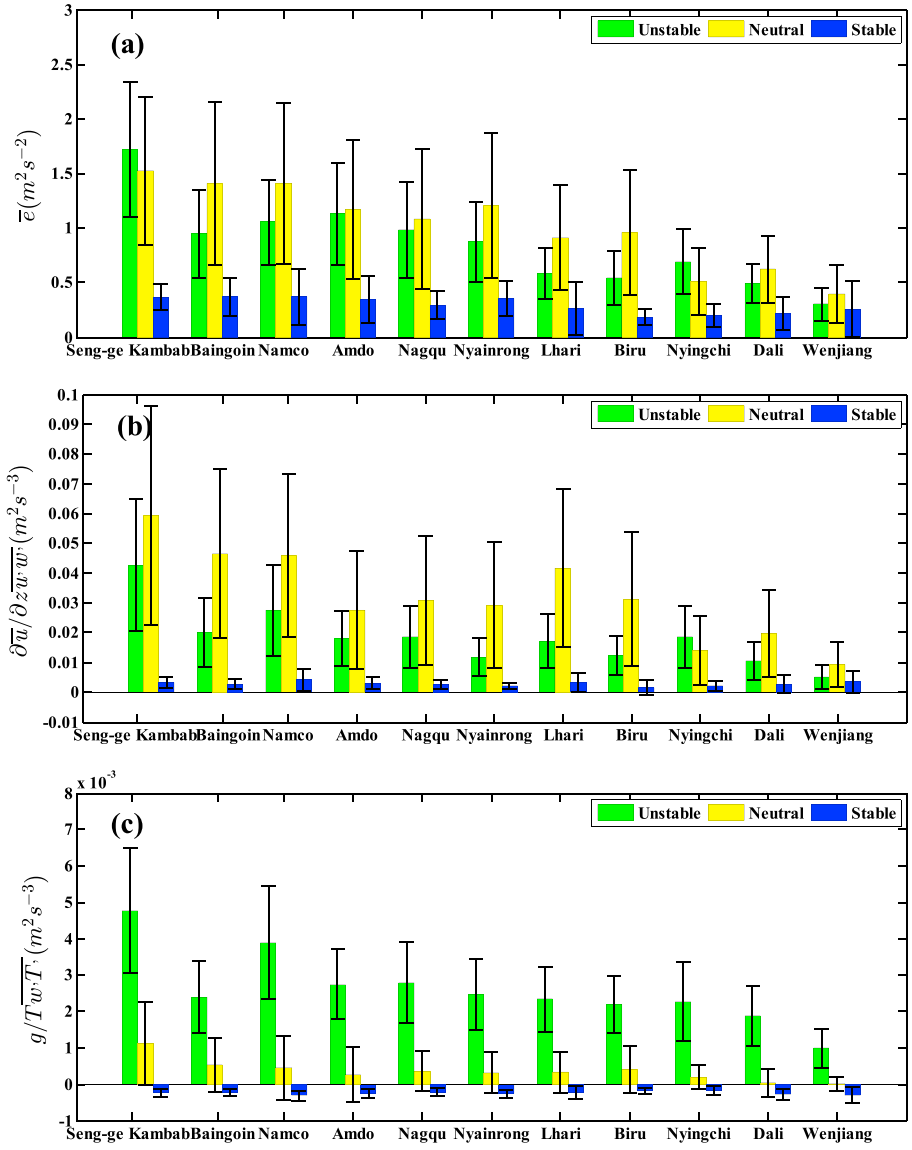

Figure 13. The variations of (a) $\bar{e}$, (b) the shear term $\left(-\partial\overline{u}/\partial z\overline{u'w'}\right)$, and (c) the buoyancy term $\left(g/T\overline{w'T'}\right)$ (for unstable, neutral, and stable) stratification in surface layer. Error bars represent standard deviation.

function of solar elevation angle and (2) the variation of underlying surface morphology which determines the distribution of *H*/*LE* (Bowen ratio). Here we use soil moisture to reflect the variation of the Bowen ratio. Based on the turbulent flux, cloud amount, and soil moisture characteristics shown in Figure 15, the 11 sites are divided into three types: (1) western TP site (Seng-ge Kambab), (2) middle TP sites (Baingoin, Namco, Amdo, Nagqu, and Nyainrong), and (3) Chengdu plain and the eastern TP sites (Lhari, Biru, Nyingchi, Dali, and Wenjiang). Cloud amount over the western TP (Seng-ge Kambab) is the least with the largest *H*, while the eastern TP sites usually have greater cloud amount with smaller *H*, and the sites on the middle TP fall in between. Both *H* and *LE* have a significant inverse relationship with cloud amount for all the sites. For example, both *H* and *LE* obviously increase during the lesser cloud amount periods (from July 25 to July 28 and from August 25 to August 29) relative to other periods at the middle TP sites. On the other hand, soil moisture increases from west to east in general. Soil moisture increases proportional to *LE*, but *H* varies inversely with it. Therefore, usually, there is a larger Bowen ratio at Seng-ge Kambab on the western TP and a smaller Bowen ratio at the sites on the eastern TP. In addition, the Bowen ratio decreases with increasing soil moisture at a given site.

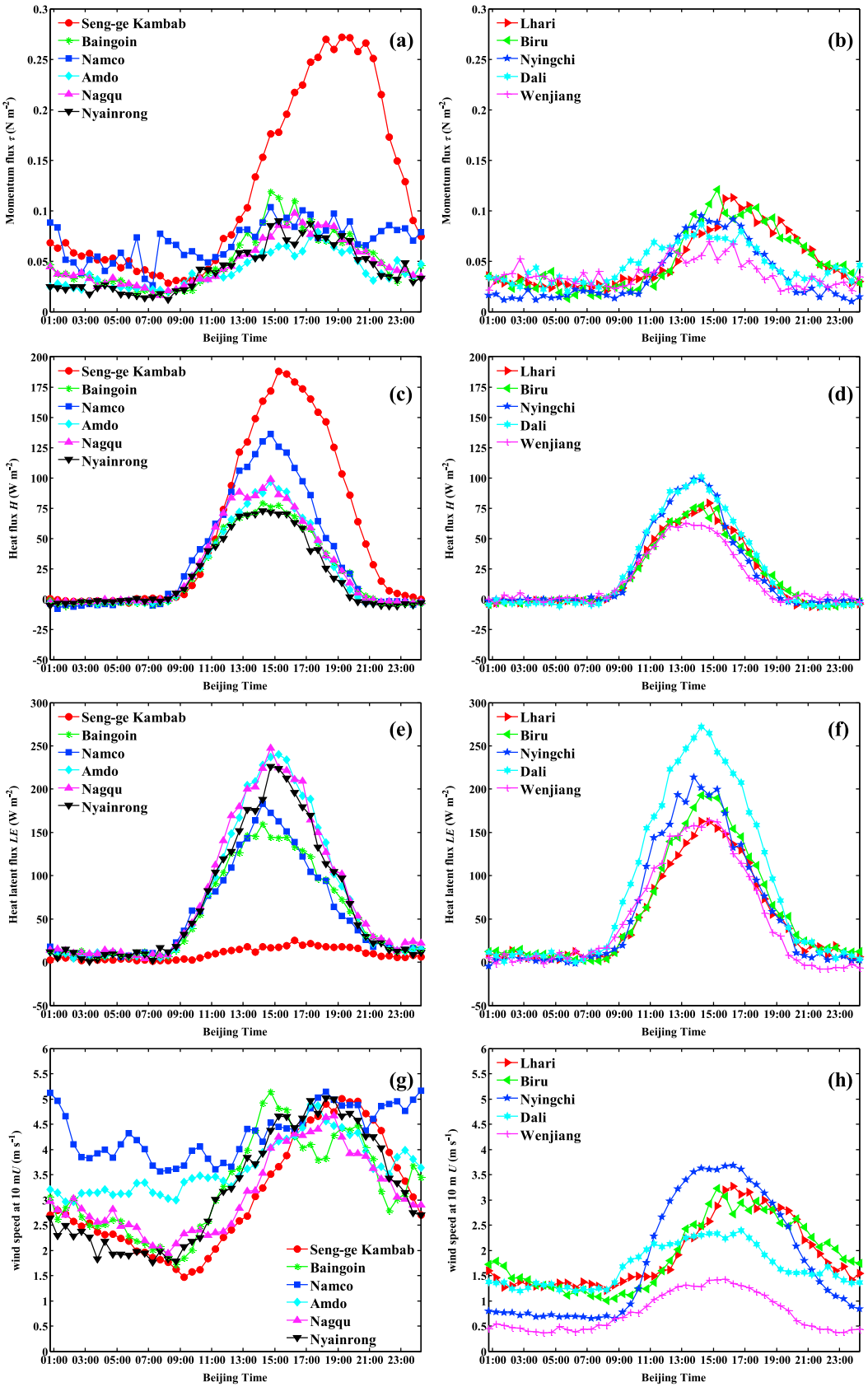

Figure 14. The diurnal variations of (a, b) momentum flux τ, (c, d) sensible heat flux H, (e, f) latent heat flux LE, and (g, h) 10 m wind speed U_{10m} for the 11 sites.

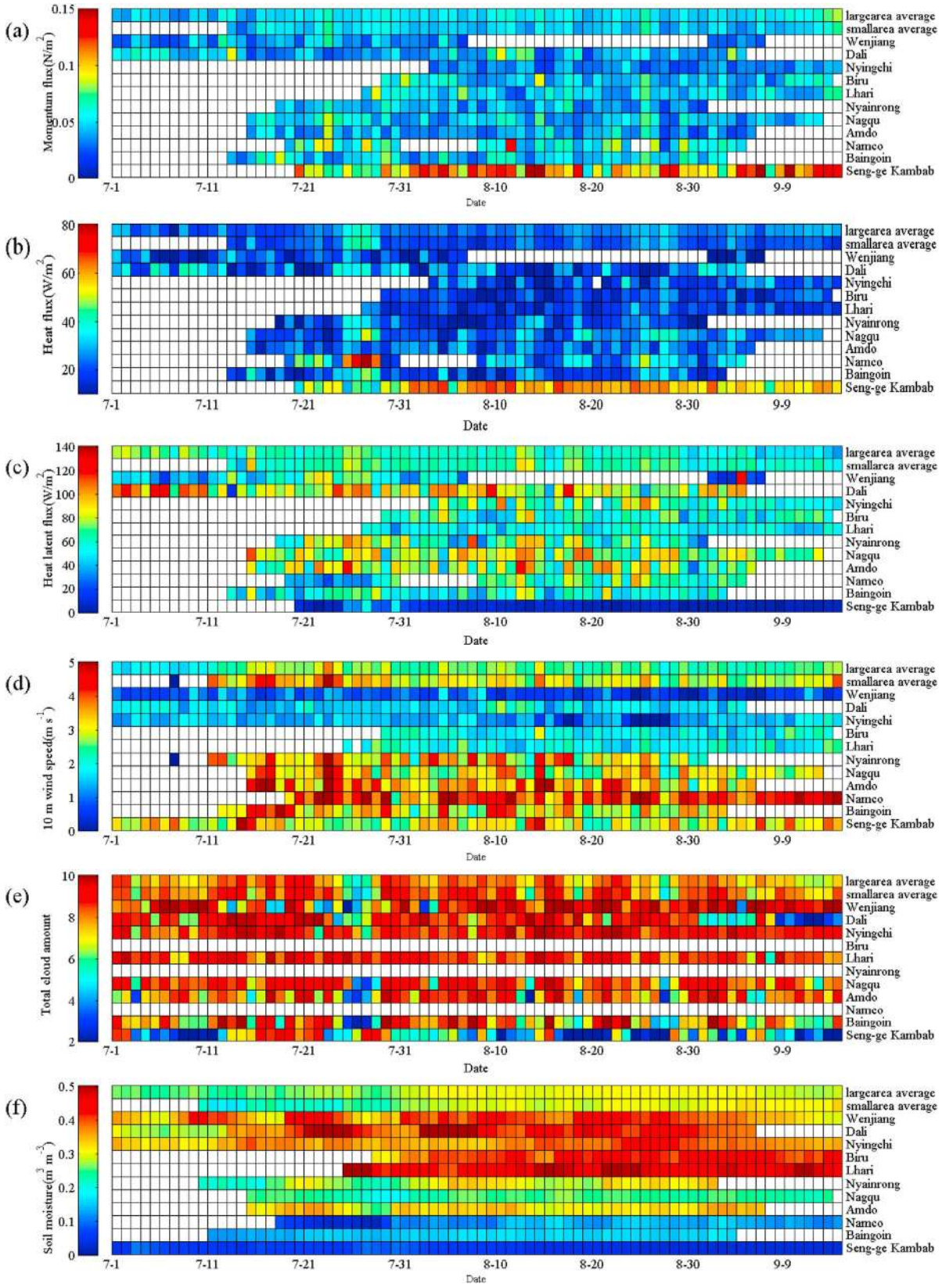

Figure 15. The daily variations of (a) momentum flux τ, (b) sensible heat flux H, (c) latent heat flux LE, (d) 10 m wind speed U_{10m}, (e) total cloud amount, and (f) soil moisture W_s for the 11 sites.

5. Conclusions

In order to understand in detail the physical process of land-air interaction over the TP and surrounding region, land surface parameters, and the turbulence characteristics in the surface layer from 11 different sites within this region are analyzed and compared. The major findings from this study are as follows.

1. The aerodynamic roughness lengths z_{0m} for the sites over the eastern TP are 1 order of magnitude larger than those within the "small network" in the middle of the TP. $kB^{-1} = \ln(z_{0m}/z_{0h})$ has obvious diurnal variation at most sites. The variations of kB^{-1} at different sites relate to meteorological conditions, the structure of the vegetation, surrounding obstructions, radiation, and soil surface resistance. Negative values of kB^{-1} can occur at night for smooth surfaces within the "small network" in the middle of the TP. Rough surfaces usually have larger kB^{-1} than smooth surfaces.
2. Surface albedo (α) is larger over the midwestern TP relative to eastern and eastern slide of TP, which is related to the drier atmosphere over the midwestern TP. α over the western arid region of the TP has significant negative correlation with soil moisture. However, a similar relationship does not exist over mid-eastern, more humid, region of the TP.
3. The averaged bulk transfer coefficients for momentum (C_D) and heat (C_H) estimated by the eddy correlation method are $2.9\times10^{-3} - 4.4\times10^{-3}$ and $2.2\times10^{-3} - 3.8\times10^{-3}$ within the "small network" in the middle of the TP. C_D and C_H at the other sites within the "large network" are $8.0\times10^{-3} - 12.6\times10^{-3}$ and $3.4\times10^{-3} - 6.0\times10^{-3}$, respectively. The results in this study show that $C_D \geq C_H$ in most cases. The relationship between the wind speed and C_D or C_H is congruous with the power function relation for unstable stratification. However, the type of function is uncertain in a stable stratification. C_D differs from C_H, and sometimes C_D does not increase monotonically with increasing instability for unstable stratification, with a maximum for weakly unstable conditions that found at (Namco, Biru, and Nyingchi).
4. Normalized wind speed variance (σ_u/u_*, σ_v/u_*, σ_w/u_*) for neutral conditions (C_{u1}, C_{v1}, C_{w1}) and temperature and humidity variance normalized by free convection scaling (C_T, C_q) follow Monin-Obukhov similarity. (C_{u1}, C_{v1}) at Wenjiang is significantly less than those over the rest of the TP and surrounding region. However, (C_{w1}, C_T) for the TP and plains sites is almost the same. C_q is larger than C_T but with unpredicted changes for different regions. The stability (z'/L) corresponding to the minimums heat flux $\left(\overline{w'T'}\right)$ for stable stratification at the TP sites is usually smaller than those of the plains sites.
5. The shear term has a significant positive correlation with $\bar{e}$ for both unstable and stable stratification. However, the buoyancy term has a significant positive correlation with $\bar{e}$ only for unstable stratification; insignificant correlations coexist for stable stratification. The shear and buoyancy terms and $\bar{e}$ over the TP are larger than that over the southeastern TP and Wenjiang (Chengdu plain). For unstable stratification, the buoyancy term both in the "large and small network" generally decreases from west to east, which is the important reason for the similar trend in $\bar{e}$. The shear term also generally decreases from west to east, but there is no obvious trend within the "small network." Overall, the larger shear and buoyancy terms over the TP could produce larger $\bar{e}$ relative to the low elevation regions especially for unstable and neutral stratification.
6. τ in the middle of the TP is larger than that over the southeastern TP and Wenjiang (Chengdu plain). Heat flux gradually decreases from western TP to the Chengdu plain. Latent heat flux increases significantly from western TP to the middle of the TP and remains almost constant from there to eastern TP. The daily variations of τ and wind speed are significantly correlated, and the same wind speed can produce more turbulence over a rough surface compared to a smooth surface. The daytime variations of both *H* and *LE* have a significant inverse relationship with cloud amount for all the sites. Soil moisture increases from west to east in general. Soil moisture increases proportional to *LE*, but *H* varies inversely with it. Therefore, usually the Bowen ratio is large at Seng-ge Kambab on the western TP and smaller Bowen ratio at the sites on the eastern TP. In addition, the Bowen ratio decreases with increasing soil moisture at a given site.

Acknowledgments

This study was supported by the China special fund for meteorological research in the public interest grant GYHY201406001, National Key Technologies R&D Program of China grant 2012BAK10B04, and the National Natural Science Foundation Of China grant 41130960. The National Center for Atmospheric Research is sponsored by the National Science Foundation. If the researchers want to access the third Tibetan Plateau Experiment for atmospheric sciences (TIPEX III) data used in this manuscript, they can contact author Yinjun Wang. E-mail: pbl_wyj@sina.cn. At the present time, the data can only be accessed from the scientific project after signing the agreement given by China Meteorological Administration.

References

Andreas, E., R. Hill, J. Gosz, D. Moore, W. Otto, and S. Sarma (1998), Statistics of surface layer turbulence over terrain with metre-scale heterogeneity, *Boundary Layer Meteorol.*, *86*, 379–408, doi:10.1023/A:1000609131683.

Beljaars, A., and A. Holtslag (1991), Flux parameterization over land surfaces for atmospheric models, *J. Appl. Meteorol.*, *30*(3), 327–341, doi:10.1175/1520-0450(1991)030<0327:FPOLSF>2.0.CO;2.

Bian, L., Z. Gao, X. Xu, L. Lu, and Y. Cheng (2002), Measurements of turbulence transfer in the near-surface layer over the southeastern Tibetan Plateau, *Boundary Layer Meteorol.*, *102*, 281–300, doi:10.1023/A:1013177629245.

Bian, L., X. Xu, L. Lu, Z. Gao, M. Zhou, and H. Liu (2003), Analyses of turbulence parameters in the near-surface layer at Qamdo of the southeastern Tibetan Plateau, *Adv. Atmos. Sci.*, *20*(3), 369–378, doi:10.1007/BF02690795.

Chen, S., M. Zhou, S. Liu, F. Qian, L. Su, L. Chen, and X. Xu (2002), Characteristics of the turbulence in the surface layer over the Plateau of western China [in Chinese], *Chin. J. Geophys.*, *45*(suppl.), 93–105.

Choi, T., et al. (2004), Turbulent exchange of heat, water vapor, and momentum over a Tibetan prairie by eddy covariance and flux variance measurements, *J. Geophys. Res.*, *109*, D21106, doi:10.1029/2004JD004767.

David, B., and G. Asner (2002), Moisture effects on soil reflectance, *Soil Sci. Soc. Am. J.*, *66*, 722–727.

Derbyshire, H. (1990), Nieuswtadt's stable boundary layer revisited, *Q. J. R. Meteorol. Soc.*, *116*, 127–158, doi:10.1002/qj.49711649106.

Feng, J., H. Liu, L. Wang, Q. Du, and L. Shi (2011), Seasonal and inter-annual variation of surface roughness length and bulk transfer coefficients in a semiarid area, *Sci. China, Ser. D*, *55*, 254–261, doi:10.1007/s11430-011-4258-2.

Högström, U. (1996), Review of some basic characteristics of the atmospheric surface layer, *Boundary Layer Meteorol.*, *78*, 215–246, doi:10.1007/BF00120937.

Katul, G., and C. Hsieh (1999), A note on the flux-variance similarity relationships for heat and water vapor in the unstable atmospheric surface layer, *Boundary Layer Meteorol.*, *90*, 327–338, doi:10.1023/A:1001747925158.

Kohsiek, W., H. A. R. de Bruin, H. The, and B. van den Hurk (1993), Estimation of the sensible heat flux of a semi-arid area using surface radiative temperature measurements, *Boundary Layer Meteorol.*, *63*, 213–230.

Li, G., T. Duan, and Y. Gong (2002), A composite study of the surface fluxes on the Tibetan Plateau [in Chinese], *Acta Meteorol. Sin.*, *60*(4), 453–460, doi:10.11676/qxxb2002.053.

Liu, H., and J. Feng (2007), Turbulent characteristics of the surface layer in Rongbuk Valley on the Northern Slope of Mt. Qomolangma [in Chinese], *Plateau Meteorol.*, *26*(6), 1151–1161.

Liu, H., and Z. Hong (2000), Turbulent characteristics in the surface layer over Gerze Area in the Tibetan Plateau [in Chinese], *Chin. J. Atmos. Sci.*, *24*(3), 289–300, doi:10.3878/j.issn.1006-9895.2000.03.01.

Liu, H., B. Wang, and C. Fu (2008), Relationships between surface albedo, soil thermal parameters and soil moisture in the semi-arid area of Tongyu, northeastern China, *Adv. Atmos. Sci.*, *25*(5), 757–764, doi:10.1007/s00376-008-0757-2.

Ma, S. (1990), The characters of the turbulent transports in the surface layer over the eastern Tibet during the summer 1986 [in Chinese], *Acta Meteorol. Sin.*, *48*(2), 210–219, doi:10.11676/qxxb1990.025.

Ma, Y., M. Menenti, R. Feddes, and J. Wang (2008), Analysis of the land surface heterogeneity and its impact on atmospheric variables and the aerodynamic and thermodynamic roughness lengths, *J. Geophys. Res.*, *113*, D08113, doi:10.1029/2007JD009124.

Mahrt, L. (1996), The bulk aerodynamic formulation over heterogeneous surfaces, *Boundary Layer Meteorol.*, *78*, 87–119, doi:10.1007/BF00122488.

Malhi, Y. (1995), The significance of the dual solutions for heat fluxes measured by the temperature fluctuation method in stable conditions, *Boundary Layer Meteorol.*, *74*(4), 389–396, doi:10.1007/BF00712379.

Moncrieff, J., J. M. Massheder, H. de Bruin, J. Elbers, T. Friborg, B. Heusinkveld, P. Kabat, S. Scott, H. Soegaard, and A. Verhoef (1997), A system to measure surface fluxes of momentum, sensible heat, water vapour and carbon dioxide, *J. Hydrol.*, *188-189*, 589–611, doi:10.1016/S0022-1694(96)03194-0.

Moncrieff, J., R. Clement, J. Finnigan, and T. Meyers (2004), Averaging, detrending and filtering of eddy covariance time series, in *Handbook of Micrometeorology: A Guide for Surface Flux Measurements*, pp. 7–31, Kluwer Acad., Dordrecht, Netherlands.

Paulson, C. (1970), The mathematical representation of wind speed and temperature profiles in the unstable atmospheric surface layer, *J. Appl. Meteorol.*, *9*(9), 857–861, doi:10.1175/1520-0450(1970)009<0857:TMROWS>2.0.CO;2.

Shimizu, T. (2015), Effect of coordinate rotation systems on calculated fluxes over a forest in complex terrain: A comprehensive comparison, *Boundary Layer Meteorol.*, *156*, 277–301, doi:10.1007/s10546-015-0027-7.

Srivastava, P., and M. Sharan (2015), Characteristics of the drag coefficient over a tropical environment in convective conditions, *J. Atmos. Sci.*, *72*, 4903–4913, doi:10.1175/JAS-D-14-0383.s1.

Stull, R. B. (1988), *An Introduction to Boundary Layer Meteorology*,666 pp., Kluwer Acad., Dordrecht, Netherlands.

Tanner, C., and G. Thurtell (1969), Anmoclinometer measurements of Reynold stress and heat transport in the atmospheric surface layer, *Res. and Dev. Tech. Rep. ECOM 66-G220F*, 82 pp., Dep. of Soil Sci., Univ. of Wisconsin, Madison.

Verhoef, A., H. Bruin, and B. Hurk (1997), Some practical notes on the parameter kB^{-1} for sparse vegetation, *J. Appl. Meteorol.*, *36*, 560–572, doi:10.1175/1520-0450(1997)036<0560:SPNOTP>2.0.CO;2.

Vickers, D., and L. Mahrt (1997), Quality control and flux sampling problems for tower and aircraft data, *J. Atmos. Oceanic Technol.*, *14*, 512–526, doi:10.1175/1520-0426(1997)014<0512:QCAFSP>2.0.CO;2.

Voogt, J. A., and C. S. B. Grimmond (2000), Modeling surface sensible heat flux using surface radiative temperatures in a simple urban area, *J. Appl. Meteorol.*, *39*, 1679–1699, doi:10.1175/1520-0450-39.10.1679.

Wang, K., J. Liu, X. Zhou, S. Michael, M. Ma, and Z. Sun (2004), Validation of MODIS global land surface albedo product using ground measurements in a semidesert region on the Tibetan Plateau, *J. Geophys. Res.*, *109*, D05107, doi:10.1029/2003JD004229.

Webb, E., G. Pearman, and R. Leuning (1980), Correction of flux measurements for density effects due to heat and water vapour transfer, *Q. J. R. Meteorol. Soc.*, *106*(447), 85–100, doi:10.1002/qj.49710644707.

Xu, X., C. Lu, X. Shi, and S. Gao (2008), World water tower: An atmospheric perspective, *Geophys. Res. Lett.*, *35*, L20815, doi:10.1029/2008GL035867.

Xu, X., T. Zhao, C. Lu, Y. Guo, B. Chen, R. Liu, Y. Li, and X. Shi (2014), An important mechanism sustaining the atmospheric "water tower" over the Tibetan Plateau, *Atmos. Chem. Phys.*, *14*, 11,287–11,295, doi:10.5194/acp-14-11287-2014.

Yang, K., T. Koike, H. Ishikawa, J. Kim, X. Li, H. Liu, S. Liu, Y. Ma, and J. Wang (2007), Turbulent flux transfer over bare-soil surfaces: Characteristics and parameterization, *J. Appl. Meteorol. Climatol.*, *47*, 276–290, doi:10.1175/2007JAMC1547.1.

Yue, P., Q. Zhang, R. Y. Wang, Y. H. Li, and S. Wang (2015), Turbulence intensity and turbulent kinetic energy parameters over a heterogeneous terrain of the Loess Plateau, China, *Adv. Atmos. Sci.*, *32*(9), 1291–1302, doi:10.1007/s00376-015-4258-9.

Zhang, J., B. Zhu, and F. Zhu (1988), *Advance of Meteorology About Tibetan Plateau* [in Chinese], 268 pp., Science, Beijing.

Zhang, Q., G. Wei, R. Huang, and X. Zeng (2002), Bulk transfer coefficients of the atmospheric momentum and sensible heat over desert and Gobi in arid climate region of Northwest China, *Sci. China, Ser. D*, *45*, 468–480, doi:10.1360/02yd9049.

Zhao, M. (1991), *Dynamics of Atmospheric Boundary Layer* [in Chinese], 350 pp., Higher Educ. Press, Beijing.

Zhou, M., X. D. Xu, L. G. Bian, J. Y. Chen, H. Z. Liu, and J. Zhang (2000), *Observational Analysis and Dynamic Study of Atmospheric Boundary Layer on Tibetan Plateau* [in Chinese], 125 pp., China Meteorol. Press, Beijing.

Zhou, M., et al. (2005), Beijing urban atmospheric boundary layer low-level dynamic and thermodynamic characteristics of the vertical and its study on the relationship between pollutant concentrations [in Chinese], *Sci. China, Ser. D*, *32*(S1), 20–30.